SALOME Quentin

M2 Astronomie, Astrophysique et Ingénierie Spatiale
Magistère de Physique d'Orsay

The Draco nebula: a diffuse molecular cloud at high Galactic latitude

Structure formation in collision in the diffuse interstellar medium

Internship supervisor:
MIVILLE-DESCHENES Marc-Antoine

Institut d'Astrophysique Spatiale, campus universitaire d'Orsay (bâtiment 209F)

The Draco nebula: a diffuse molecular cloud at high Galactic latitude

Abstract:

The Draco nebula is a high Galactic latitude interstellar cloud. Its formation is still a matter of debate. It might have been formed by the collision between a high-velocity cloud and gas of the Galactic plane. In order to better understand the formation of the Draco nebula, *Herschel* observations were obtained with the instrument SPIRE. Combined with *IRAS* and *Planck*, and HI-21 cm data, we were able to study the gas dynamics and the properties of the nebula.

The high-resolution of the 250 μm SPIRE map reveals Rayleigh-Taylor (RT) instability structure at the hypothetic shock-front. The analysis of the RT instability structure allowed us to estimate the density of the two colliding fluids. In addition, dense clumps are observed in the RT instability structure.

Using a clump finder algorithm, we found that 1/8 of the Draco nebula mass is located in the clumps and, the clump mass function follows a power law. The power law index is compatible with the one of non self-gravitating clumps observed in molecular clouds like Taurus or Orion. On the other hand, it is a factor of 3-4 smaller than the slope of the core and initial mass function. This result highlight the necessity of numerical simulations. Indeed, the involved processes (turbulence, magnetic field, heating/cooling processes) are complex and not well understood.

Résumé:

La nébuleuse Draco est un nuage interstellaire à haute latitude galactique. Sa formation est encore sujet à débat. Il pourrait avoir été formé par la collision d'un nuage à haute vitesse avec le gaz du plan galactique. Pour mieux comprendre la formation de la nébuleuse Draco, des observations *Herschel* ont été obtenues avec l'instrument SPIRE. Combinées avec les données *IRAS* et *Planck*, ainsi que des données HI-21 cm, nous avons pu étudier la dynamique du gaz et les propriétés de la nébuleuse.

La haute résolution de la carte SPIRE à 250 μm révèle une structure due à l'instabilité de Rayleigh-Taylor (RT) au niveau du front de choc supposé. L'analyse de la structure de RT nous a permis d'estimer la densité des deux fluides qui sont entrés en collision. De plus, des "clumps" denses sont observés dans cette structure.

En utilisant un algorithme pour détecter les clumps, nous avons trouvé que 1/8 de la masse de la nébuleuse Draco se situe dans les clumps, et que la "clump mass function", c'est-à-dire la distribution en masse des clumps, suit une loi de puissance. L'indice de cette loi de

puissance est compatible avec celle de clumps non auto-gravitants observés dans des nuages moléculaires comme Taurus ou Orion. D'un autre coté, cet indice est 3-4 fois plus faible que la pente des "core" et "initial mass function". Ceci met en lumière la nécessité d'utiliser des simulations numériques. En effet, les processus mis en jeu (turbulence, champ magnétique, processus de chauffage/refroidissement) sont complexes et mal compris.

Contents

Introduction

Our Galaxy, as all galaxies, is an open and dynamical system. Matter is constantly arriving on the galactic disk. Part of this gas is the result of the galactic fountain. Hot gas rises into the halo from stellar wind and supernovae. Then, it condenses into cold clouds and returns to the disk due to gravity [1]. The other part of the infall matter comes from intergalactic space [1], either gas stripped from satellite galaxies or gas from the inter-galactic medium (IGM).

This extragalactic gas enters the galaxy through the galactic halo [1]. It allows to maintain a roughly constant star-formation rate over the galaxy life [2].

The high-velocity clouds (HVC) in our Galaxy have been considered as possible direct evidence for extragalactic infalling gas. In addition, the intermediate-velocity clouds (IVC) are closer to the Galactic layer. Most of them are part of the Galactic fountain, but some should be HVCs that interact with the disk. It is now clear that IVCs and HVCs are a halo population of our Galaxy [2]. The Galactic fountain scenario can explain both upward- and downward-moving IVCs.

Clouds that are part of the Galactic fountain should have metallicities similar to the solar one. Clouds that are composed of material from satellite galaxies should have metallicities similar to the metallicity of the original galaxies. Finally, gas from the IGM, that has never cycled in any galaxy, should have a very low metallicity.

Because of the importance of the process for galaxy evolution, many studies have been dedicated to the disk-halo interaction. One example is Kwak et al. [3] who modelled and studied the dynamical evolution of gas clouds after they form in the halo and begin to fall toward the Galactic plane. They successively change the cloud density and the magnetic field. As expected, these authors found that interstellar medium's (ISM) resistance is more important when the magnetic field is strong and perpendicular to the motion of the cloud.

A cloud is more likely to accelerate to HVC-class velocities if it is initially dense enough to overcome the interaction with the ambient ISM [3]. This interaction depends on the magnetic field in the Galactic halo. If the magnetic field is parallel to the Galactic plane, the falling cloud would be most effectively decelerated.

Kwak et al. found that an initial density $n = 0.1\, cm^{-3}$ is large enough to get HVCs if the ambient magnetic field strength is $\leq 1.3\, \mu G$. If the density is 10 times smaller, the cloud reaches HVC velocities only if the magnetic field is absent or parallel to the cloud's motion.

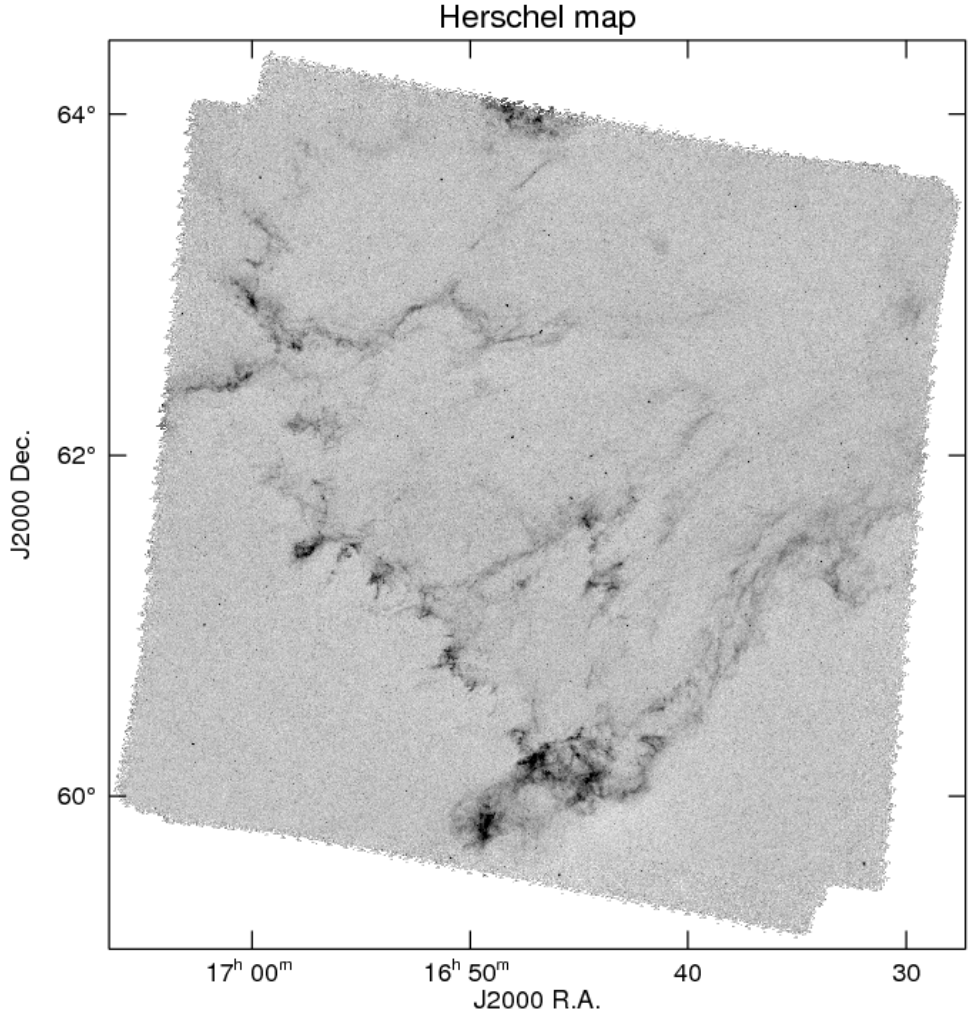

Figure 1: Intensity map at 250 μm of the Draco nebula by the *Herschel* Space Observatory. Brightness scale is inverted.

During this internship, I studied the Galactic fountain scenario and the formation of structures resulting from the collision of diffuse gas. The study is based on the analysis of *Herschel*-SPIRE observations of the Draco nebula (figure 1). The map presents a diffuse cloud with bright filamentary structures. Also, low declinations show a bright interface with small structures (clumps).

With the instrument SPIRE, we have a very good resolution (17.6″ resolution). This allows us to study small scale structures in more details, especially the clumps. Using dust emission, we were able to estimate their mass and the total amount of mass they contain. Thus, we may go deeper in the formation scenario of Draco, and especially study if the gas that enters the disk is in the cold (CNM) or warm neutral medium (WNM) phase.

In the first part of this report, I will present the characteristics of the Draco nebula. I will then explain how I created a column density map using *Herschel*, *Planck* and *IRAS* data. In a third part, I will study the Rayleigh-Taylor instability in the case of the Draco nebula. Finally, I will analyse the small scale structures, and compare the results with published results.

1 Characteristics of the Draco nebula

The Draco nebula (figure 1) is a diffuse IVC at high Galactic latitude ($l \approx 91°$,$b \approx 38°$). It is located above the Galactic plane and is probably illuminated and excited by radiation from the Galactic disk [4]. In the local standard of rest (LSR), the mean velocity of the Draco nebula is $-23.7 \pm 1.8\, km.s^{-1}$. It is one of the rare example where we can study the nature of the gas of the halo entering the disk.

The Draco nebula was first observed with 21-cm observations by Goerigk et al. [5]. Overlaying observations made by the Palomar Observatory Sky Survey (POSS) with the 21-cm brightness temperature, they observed that the cloud coincides with a faint diffuse nebula seen in the optical.

1.1 Dynamics

1.1.1 Velocities

The structure of the HVC and the IVC components can be estimated using HI 21-cm data. The radial velocities are determined with the Doppler effect of the spectral line. The HI data are a two dimension array, where each element contains a spectrum as figure 2. Those spectra show three shifted lines corresponding to HI in the LVC (low-velocity cloud - the gas in the solar neighborhood), IVC and the HVC components. By selecting ranges of velocity channels, one may get maps for each components.

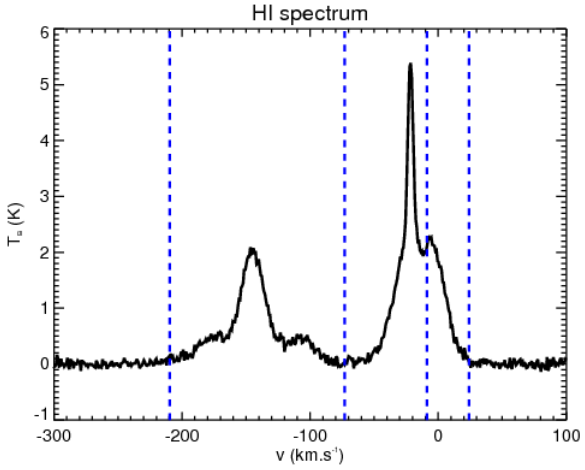

Figure 2: 21-cm spectrum for the Draco nebula. The blue dash lines show the LSR velocity ranges used to estimate IVC and HVC components. These ranges are relevant with the spectrum lines.

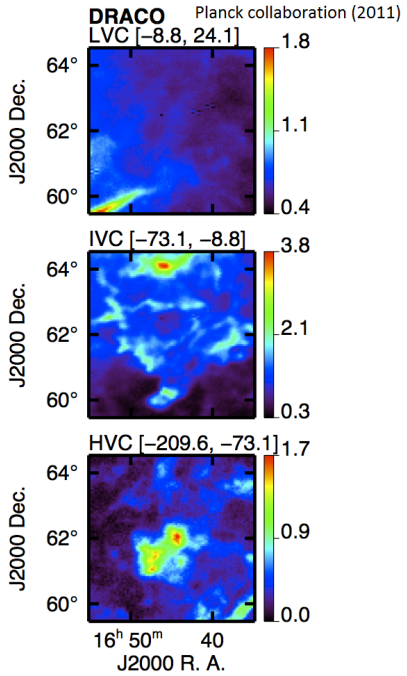

Figure 3: HI column density maps in units of $10^{20} cm^{-2}$ for the Draco nebula. *Up to down*: LVC, IVC and HVC components. These maps were computed by Planck collaboration [6] using data from the Green Bank Telescope.

A previous study from Planck collaboration [6] separated the three components. For the Draco nebula, they computed HI column density maps shown in figure 3. For our study, we are only interested in the IVC and the HVC. Both components seem to be located one behind the other. This is an argument in favor of a formation scenario which involves a collision between a HVC and the WNM of the Galactic disk (LVC).

Using the same velocity ranges than Planck collaboration [6] (in blue dash lines in figure 2), I made maps of average velocity and velocity dispersion (figure 4) using formulae from [7]: $\langle v \rangle_i = \frac{\sum T_B(v)v}{\sum T_B(v)}$ and $\sigma_i^2 = \frac{\sum T_B(v)v^2}{\sum T_B(v)} - \langle v \rangle_i^2$. Then, we calculated the mean velocity (resp. the error over the mean velocity) of a component as the average (resp. the standard deviation) of the mean velocity over all the pixels: $\langle v \rangle = \sum_i \langle v \rangle_i$ and $(\delta \langle v \rangle)^2 = \sum_i \langle v \rangle_i^2 - \langle v \rangle^2$. We did the same thing for the velocity dispersion.

Applying these equations, we found a mean velocity $-23.7 \pm 1.8\, km.s^{-1}$ (resp. $-141.8 \pm 12.6\, km.s^{-1}$) with a velocity dispersion $10.7 \pm 1.8\, km.s^{-1}$ (resp. $29.7 \pm 5.8\, km.s^{-1}$) for the IVC (resp. HVC) component.

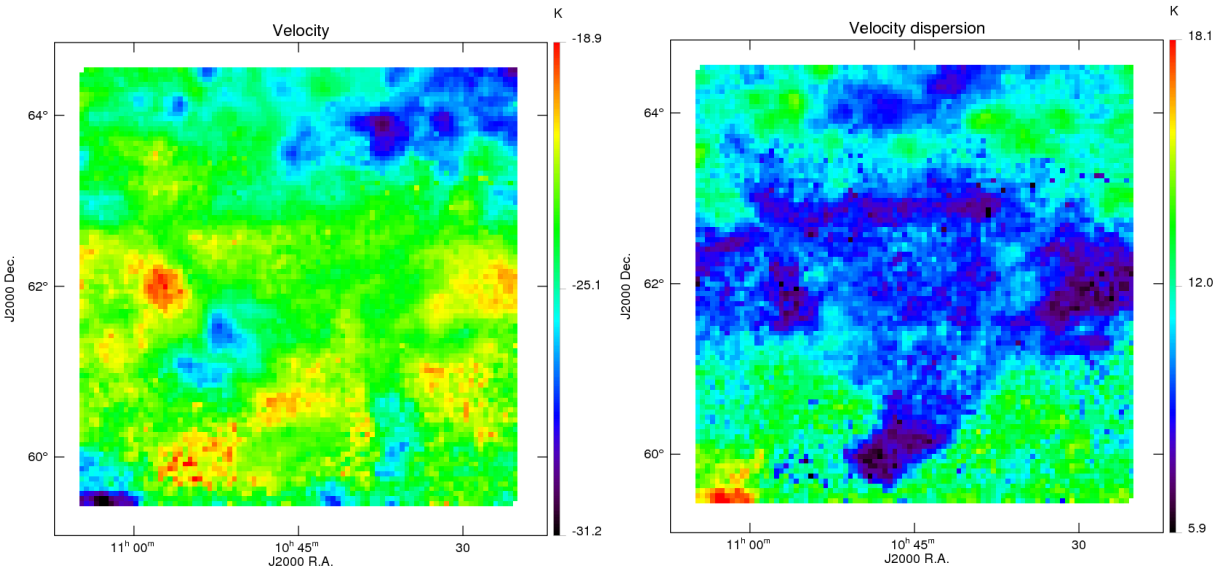

Figure 4: Mean velocity (left) and velocity dispersion (right) maps for the IVC component of the Draco nebula obtained from 21-cm GBT data.

LSR velocities are radial velocities. Assuming the movement to be purely perpendicular to the Galactic plane [8], velocities are $v = v_{LSR}/\sin b$. Therefore, the mean velocity and velocity dispersion are $\langle v \rangle = -38.5 \pm 2.9\, km.s^{-1}$ and $\sigma = 17.4 \pm 2.9\, km.s^{-1}$ (resp. $\langle v \rangle = -230.3 \pm 20.5\, km.s^{-1}$ and $\sigma = 48.2 \pm 9.4\, km.s^{-1}$) for the IVC (resp. HVC) component.

1.1.2 Structures

In 1983, Goerigk et al. [5] identified a front-like structure which coincides with the boundary of the Draco nebula. This boundary exhibits a normal velocity gradient. These authors hypothesized a shock-front with Rayleigh-Taylor (RT) instability.

In 1985, Mebold et al. [4] carried CO-observations ($^{12}CO\ \lambda 2.6mm$ and $^{13}CO\ \lambda 2.7mm$) of the brightest part of the nebula. The ^{12}CO-line brightness distribution shows four CO-clumps

centered at the positions listed in table 1. Those clumps are represented on SPIRE map (figure 5). The names of these clumps were selected based on the cloud morphology.

Name	Position		Size		Velocity	Velocity gradient
(1)	(2)		(3)		(4)	(5)
	l	b	Δl	Δb	V_{LRS}	ΔV
Fang	91°11'	36°59'	5'	8'	-24.2	0.3
Wart	89°32'	38°24'	15'	15'	-23.3	0.1
Drop	90° 1'	38°35'	5'	5'	-24.0	0.2
Horn	89°55'	38°55'	25'	20'	-23.7	0.1

Table 1: Observational parameters of the CO-clumps in the Draco nebula [4]. The velocities are in $km.s^{-1}$ and the gradients are in $km.s^{-1}/arcmin$.

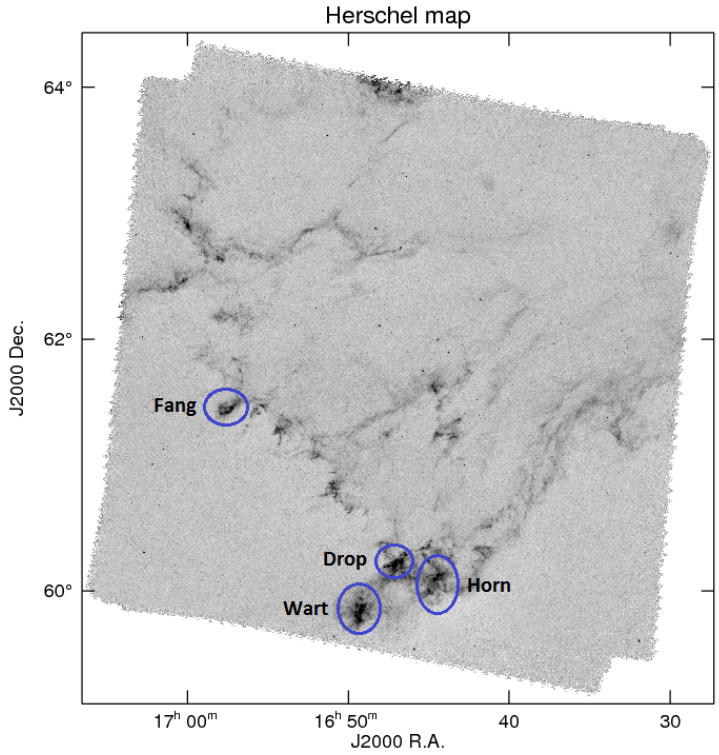

Figure 5: Position of the CO-clumps observed by Mebold et al. [4], represented on the 250 μm SPIRE map.

1.1.3 Scenario of the formation

The Draco nebula was studied for a long time and we now have a scenario which may explain its formation. Because of the spatial correspondance with the HVC, the cloud could originate from the IGM. This gas is falling toward the Galactic disk and collided with the WNM of the disk.

There is indeed evidence that the Draco nebula is falling towards the Galactic plane, being decelerated by interaction with Galactic gas: (1) Radial velocities are negative in the LSR; (2) the velocity gradient is positive at the boundary; (3) for the CO-clump 'Fang', dust presents

a filamentary morphology [9] and (4) Kalberla et al. [10] observed a HI "stream" which is probably formed by an inelastic collision.

This favored scenario of a collision between a HVC and the WNM of the Galactic disk is schematised on figure 6.

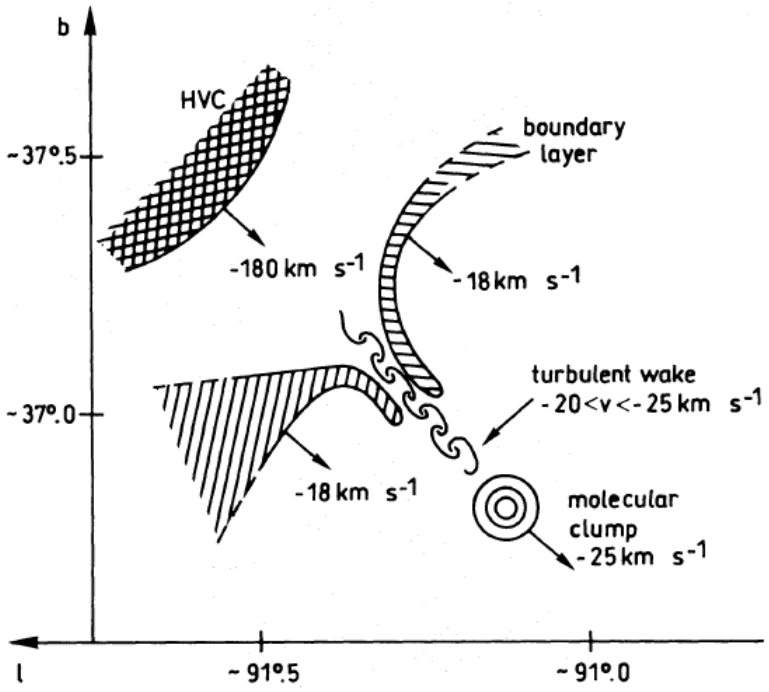

Figure 6: Sketch of the collision scenario described in [9]. The velocities are radial velocities with respect to the local standard of rest.

1.2 Molecular content

At the boundary of the nebula, emission from molecules such that CO, H_2CO and NH_3 have been detected in the brightest clumps [4]. The Draco nebula is one of the two IVCs in the disk-halo interface that show CO emission [11]. Estimates from dust and X-ray data indicate a total hydrogen column density of $N_H \sim 3 \times 10^{20}\, cm^{-2}$ [12]. In the brightest part of the nebula, the x_{CO} factor is 10 times smaller than usual ($0.17 \times 10^{20}\, cm^{-2}\, (km.s^{-1})^{-1}$) [12], indicative of a high CO abundance, potentially caused by a shock.

Using star counts, Goerigk et al. [5] have estimated extinction. Plotting the column density N_{HI} versus the relative colour excess $\Delta E(B-V)$, they found that the total hydrogen column density is about 10 times higher than the HI column density. The missing nuclei are probably in molecular form, which is unusual for such diffuse clouds.

Using observations of the CO (J=1-0) transition, Magnani et al. [13] observed molecular cloud at high Galactic latitudes with ratios $N(H_2)/N(HI)$ equal to 2-3, up to more than 9. For the Draco nebula, they found extinction $A_V = 0.7$, which corresponds to a hydrogen column density of $N_H \approx 1.32 \times 10^{21}\, cm^{-2}$.

The formation of molecules in dense parts of shocks is not unexpected. Koyama and

Inutsuka [14] have done one-dimensional hydrodynamic calculations for the propagation of a strong shock wave into WNM and CNM. They found that the shock propagation can produce a thin and dense H_2 layer by the thermal instability inside the shock-compressed layer. They also predict that the thermally collapsed layer will fragment into small molecular clouds.

1.3 Distance estimate

To determine the position of the Draco nebula in the Galactic frame, it is important to know the distance. Moreover, distance is important to estimate structures size and mass.

In 1985, Mebold et al. [4] infered the distance using a star count deficit technique with the star counts published by Goerigk et al. [5] and a model of the distribution of stars. The star count deficit $\Delta N = N_{off} - N_{on}$ is the difference of star counts at an unabsorbed reference field (N_{off}) and at the dust cloud. It is given by $\frac{\Delta N}{N_{off}} = 0.11 \pm 0.02$, where N_{off} is the number of stars counted off the nebula. These authors concluded that $d \geq 800\,pc$.

In 1986, Goerigk and Mebold [15] derived the distance of the Draco nebula from UBV photometry. They observed 95 stars located in the brightest part of the nebula, up to a distance of $\sim 1\,kpc$. They derived distances measuring $B-V$ and $U-B$ colors, and estimating the spectral types and absolute magnitudes for stars. The largest distances they found are $700 < d < 1100\,pc$.

In 1991, Lilienthal et al. [16] pointed that the star count method has many potential biases. The uncertainty on the stellar density distribution and the extinction may cause a distance uncertainty up to a factor of 2. Those author concluded that the most reliable method to estimate the distance is to look for absorption in spectra of stars with known distances.

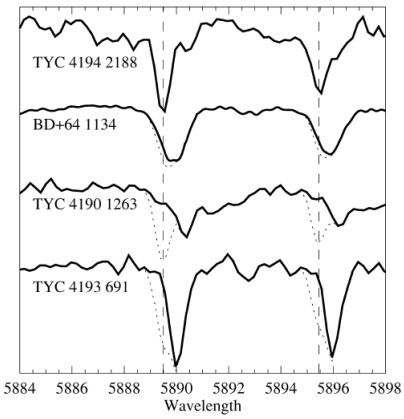

Figure 7: Spectra for the four most distant stars (thick lines) showing both stellar and interstellar sodium absorption features.

Star	Spectra type	Distance (pc)
TYC 4194 2188	A6 V	618^{+243}_{-174}
BD +64°1134	F5 V	382^{+155}_{-110}
TYC 4190 1263	F5/G0 V	463^{+192}_{-136}
TYC 4193 691	G0 V	252^{+104}_{-74}

Table 2: Spectrum analysis results from [17] for the four most distant stars.

In 1998, Gladders et al. [17] observed eight stars along the line of sight toward the Draco nebula at the sodium doublet. Those stars are blue ($B-V < 0.4$) and relatively faint ($V > 9.0$). They expected such stars to show a relatively strong sodium absorption feature. One of these stars (TYC 4194 2188) shows an unresolved absorption feature at Draco's systemic velocity

(figure 7), which means it is located behind the cloud. The other stars are in front of the Draco nebula.

The four stars have been classified and, the derived spectral class and the absolute magnitude calibration were used to assign distance to each star (Table 2). They have considered several independent sources of error in this distance estimate, including the error in the V-magnitude, and an assumed classification error of plus or minus one spectral class. The background star and the most distant foreground star set constraints on the distance: $463^{+192}_{-136} \leq d \leq 618^{+243}_{-174}\, pc$.

As can be seen from previous studies, estimate distances is a complex task. In the following, we will adopt a distance of $600\, pc$. However, distance is an important source of uncertainty for our study. At the latitude of Draco, a distance $d = 600\, pc$ corresponds to a height above the Galactic plane of $z \approx 370\, pc$. For the WNM, the half width at half maximum (HWHM) in the Galactic disk is $265\, pc$ [18], indicating that Draco is in interaction with the Galactic diffuse ISM.

1.4 Aim of the internship

We will use *Herschel* data to study the structure of the Draco nebula, in relation with the gas dynamics. We aim at better understanding the formation scenario of the Draco nebula, and studying the structure formation processes (shock, RT instability,...) in a cloud collision within diffuse interstellar medium (ISM).

Contrary to cold cores, the formation of the dense structures seen here is not due to gravity. During a strong shock, density locally increases, forming small scale structures. These structures are located along fingers of the RT instability.

First, I computed a map of total hydrogen column density in the Draco nebula with the *Herschel*-SPIRE dust emission maps and a model for big dust grains emission. The model was computed using *IRAS* and *Planck* data of temperature, and allowed us to check the consistency of *Herschel* data. Then, I estimated the total hydrogen column density from the $250\, \mu m$ SPIRE map, applying a simple relation between dust optical depth and hydrogen column density.

In a second time, I focused on the RT instability. Using a relation between the RT instability typical length, the local gravitational acceleration and the Atwood number, I estimated the density ratio between the Galactic disk and the HVC at the origin of the formation of Draco.

Finally, I studied smale scale structures in details. We have extracted the molecular clumps from the SPIRE and column density maps with the extraction code *GetSources*. Assuming all the clumps to be at the same distance ($600\, pc$), we could draw the mass and density distributions of the clumps.

2 Column density

The goal here is to obtain a map of total hydrogen column density (or dust optical depth) at the angular resolution of *Herschel*-SPIRE (17.6″ at 250 μm).

2.1 Principle

To make a map of column density, we rely on a modelling of the dust spectral energy distribution (SED), i.e. the brightness as a function of the wavelength. For big dust grains, the SED follows a "modified black-body":

$$\boxed{I_\nu = AB_\nu(T)\left(\frac{\nu}{\nu_0}\right)^\beta} \tag{1}$$

where A is the amplitude, $B_\nu(T)$ is Planck's law, and $\left(\frac{\nu}{\nu_0}\right)^\beta$ comes from models for big dust grains. At high Galactic latitude, β has a median value of 1.8 [19]. From equation 1 in the optically thin case, the dust optical depth τ_ν is defined as:

$$\tau_\nu = \frac{I_\nu}{B_\nu(T)} = A\left(\frac{\nu}{\nu_0}\right)^\beta = (N_H\, \mu m_H\, r\kappa_0)\left(\frac{\nu}{\nu_0}\right)^\beta \tag{2}$$

where N_H is the H-nuclei column density, μm_H is the mean mass of gas particles, r is the gas-to-dust ratio and κ_0 is the opacity. For a given wavelength, for instance $\lambda = 250\,\mu m$, the optical depth is proportional to the total hydrogen column density: $\tau_{250} \propto N_H$.

Because the PACS data for the Draco nebula are unusable, we rely on the model of the big dust grains emission based on lower resolution *IRAS* and *Planck* data (5′) to estimate dust temperature. We estimate τ_ν using the 250 μm SPIRE map for I_ν (17.6″ resolution) and the temperature map obtained from the *Planck+IRAS* data fit (5′ resolution) made by Planck collaboration (2013, in preparation), publicly available on the *Planck* archive. We assume the temperature fluctuations to be negligeable at scales smaller than 5′.

2.2 *Herschel*-SPIRE maps calibration

In order to use the 250 μm SPIRE map to estimate the column density, we first evaluated the quality of the map calibration by comparison with the prediction of the *Planck+IRAS* model.

2.2.1 *Herschel* observations model

Using the model of the dust emission based on *Planck* and *IRAS* data (*Planck* archive), we estimated the emission in each *Herschel*-SPIRE bands at 250 μm, 350 μm and 500 μm. For each pixel of the map, we computed the dust SED (equation 1). Then, the model was convolved with the *Herschel* spectral response and converted to $MJy.sr^{-1}$ using the *IRAS* convention

$\nu I_\nu = cte$. It corresponds to applying a color correction factor cc [20] such that $I_{\nu_0}(actual) = I_{\nu_0}(obs)/cc$, where $I_{\nu_0}(actual)$ is the actual specific intensity of the sky at frequency ν_0, $I_{\nu_0}(obs)$ is the corresponding value obtained with *Herschel* and ν_0 is the nominal frequency of the considered band. With these definitions, the color correction factor is given by equation 3.

$$cc = \frac{\int (I_\nu / I_{\nu_0})_{actual} R_\nu \mathrm{d}\nu}{\int (\nu_0/\nu) R_\nu \mathrm{d}\nu} \qquad (3)$$
$$\frac{I_\nu}{I_{\nu_0}} = \frac{B_\nu(T)\nu^\beta}{B_{\nu_0}(T)\nu_0^\beta}$$

where $(I_\nu/I_{\nu_0})_{actual}$ is the actual specific intensity of the sky normalized to the intensity at frequency ν_0 and R_ν is the spectral response of the SPIRE instrument.

Planck+IRAS data give the actual intensity of the sky so we multiply them by the color correction factor in order to obtain the dust emission model in the *Herschel*-SPIRE 250 μm band.

2.2.2 Calibration

To estimate the *Herschel*-SPIRE maps calibration, one must first decrease the *Herschel* maps resolution, as the map from the model have the IRAS/Planck resolution. To do this, we convolved *Herschel* maps with a two dimension gaussian. The gaussian standard deviation is calculated with the initial and final resolutions: $\sigma = \sqrt{\sigma_f^2 + \sigma_i^2}$. For example, if $\lambda = 250\,\mu m$, one has $\sigma = \frac{\sqrt{(5')^2+(17.6'')^2}}{2.354}$, where the factor 2.354 is the ratio between the standard deviation and the full width at half maximum (FWHM).

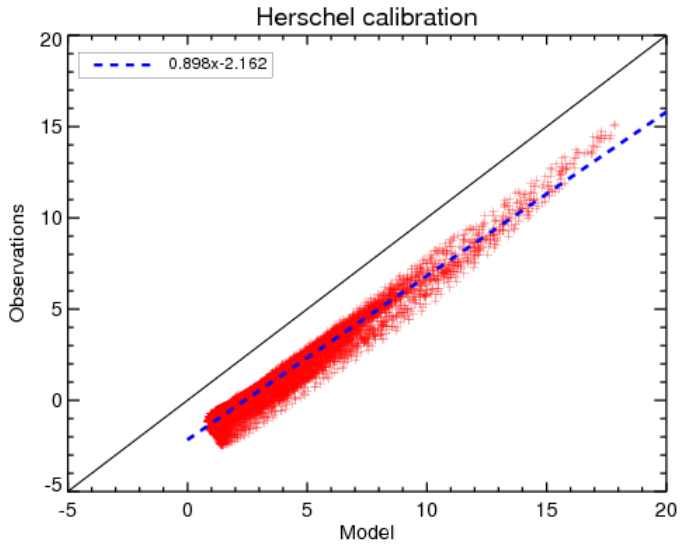

Figure 8: Intensity of the convolved 250 μm *Herschel* map versus the intensity of the dust emission model from *Planck* and *IRAS*. The slope gives the gain and the intercept is the offset.

The convolved map may now be compared with the model map. Drawing the intensity of the *Herschel* map versus the intensity of the model (figure 8), and fitting a linear polynomial, one gets the flux offset (the intercept) and the gain (the slope). The observed intensity $I_\nu(obs)$

is estimated applying equation 4:

$$I_\nu(obs) = \frac{I_\nu^H - offset}{gain} \tag{4}$$

where I_ν^H is the *Herschel* data. In the following, we will use $I_\nu(obs)$ to compute the hydrogen column density.

2.3 Results

The calibrated *Herschel*-SPIRE 250 μm map can now be converted in column density applying a conversion factor. We will get maps of hydrogen column density with SPIRE resolutions (17.6″, 23.9″ and 35.1″ for $\lambda = 250\,\mu m$, $350\,\mu m$ and $500\,\mu m$ respectively).

To determine optical depth, equation 2 must be slightly modified to take in account the color correction:

$$\tau_\nu = \frac{I_\nu / cc}{B_\nu(T)}$$

Using the map of dust temperature from the Planck/IRAS model, we first derived the map of the Planck's law $B_\nu(T)$. Dividing the calibrated map by maps of the color correction factor and the black-body, we obtain a map of dust optical depth.

In 1996, Boulanger et al. [21] studied the correlation between gas and dust in high Galactic latitude medium. They found a relation between optical depth and column density. They show that the dust emission cross-section $\sigma_e = \frac{\tau_\nu}{N_H}$ is:

$$\frac{\tau_\nu}{N_H} = 1.0 \times 10^{-25} \left(\frac{\lambda}{250\,\mu m} \right)^{-2} cm^2$$

Using *Planck* and *IRAS*, Planck collaboration (2013, in preparation) found that, at high Galactic latitudes, the dust emission cross-section is given by:

$$\frac{\tau_\nu}{N_H} \sim 8.0 \times 10^{-27} \left(\frac{\nu}{353\,GHz} \right)^{\beta} cm^2 \tag{5}$$

Applying equation 5, we convert the map of τ_ν to total hydrogen column density (figure 9). Comparing with that of HI column density computed by Planck collaboration [6] (figure 10), we deduced that the Draco nebula is mostly composed of molecular hydrogen as expected. Indeed, the maximum hydrogen column density N_H is about 10 times larger than the HI column density.

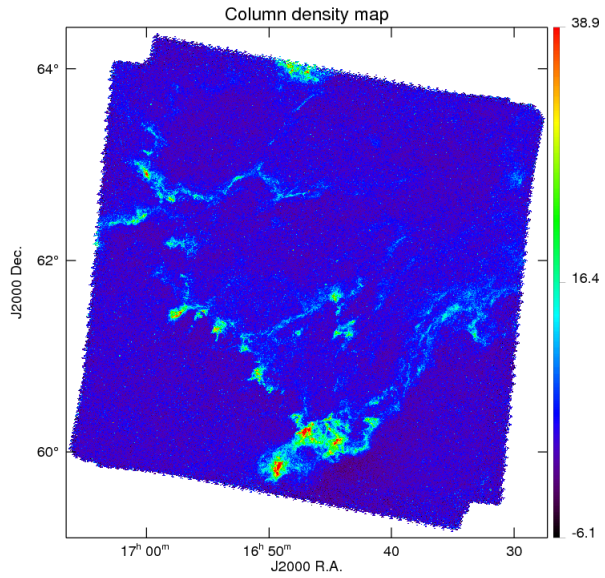

Figure 9: Hydrogen column density maps in units of $10^{20}\ cm^{-2}$ for the Draco nebula. This map was computed using *Herschel* and *Planck+IRAS* data.

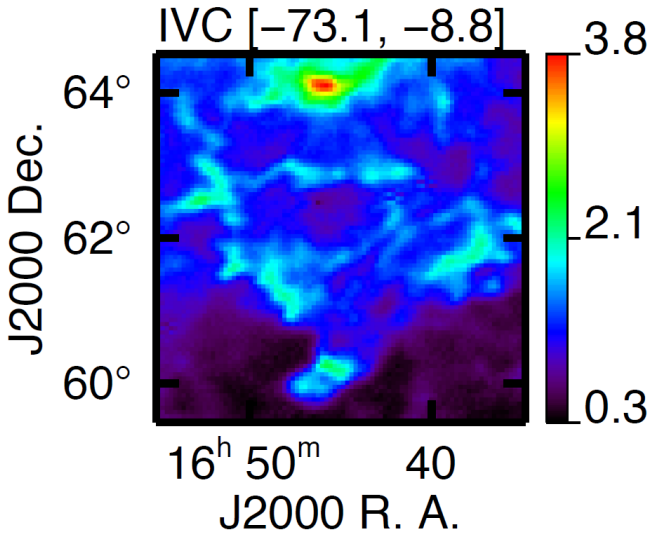

Figure 10: HI column density maps in units of $10^{20}\ cm^{-2}$ for the Draco nebula. This map was computed by Planck collaboration [6] using data from the Green Bank Telescope.

Focusing on the molecular clump called 'Fang' by Mebold et al. [4], we find an average hydrogen column density of $\langle N_H \rangle = 2.2 \pm 0.1 \times 10^{21}\ cm^{-2}$. To do this, we selected an ellipse centred around $(l = 91°11', b = 36°59')$ with an apparent size $(\delta RA, \delta Dec) = (3.5', 2.5')$.
The value is ~ 3 times smaller than the value found by Rohlfs et al. [9] on the same area using ^{13}CO data (see part 1.2). This factor may come from the value of the emission cross-section σ_e or, the ratio $X13CO$ between ^{13}CO and hydrogen column density used by Rohlfs et al.

The work presented in this part will then be applied to characterise the sources which will be extracted from the SPIRE maps (cf. part 4).

3 Rayleigh-Taylor instability

One of the most striking feature of the *Herschel* observations of the Draco nebula is the structure of the shock front that shows periodic half shells that are similar to structures produced in Rayleigh-Taylor instability (RT). In this section, we test this hypothesis.

Consider two distinct fluids in pressure equilibrium accross a common interface. This interface can be destabilized by sources of acceleration. RT instability occurs when two fluids of different densities are accelerated towards each other. As the fluids cannot interpenetrate freely, bubbles of light fluid rise into the heavy fluid forming finger structures. This is the case for an incompressible fluid but, it appears that similar structures appear in compressible fluids, like supernovae remnants.

3.1 Hydrodynamics equations

Hydrodynamics is governed by 3 equations. The equation of continuity (6) expresses the mass conservation: the change of the mass within a volume is given by the fluid outflow across the boundary. The Navier-Stokes equation (7) is the equation of motion: the momentum contained in a volume changes with the external forces acting on the fluid elements and the stresses acting on the boundary. Equation 8 expresses the thermal equilibrium.

$$\frac{\partial \rho}{\partial t} + \vec{\nabla}.(\rho \vec{v}) = 0 \tag{6}$$

$$\frac{\partial \rho \vec{v}}{\partial t} + \left(\vec{v}.\vec{\nabla}\right)(\rho \vec{v}) = -\vec{\nabla}P + \vec{\nabla}.\vec{\vec{\tau}} + \rho\overrightarrow{F_{ext}} \tag{7}$$

$$\frac{\partial e}{\partial t} = n\Gamma(T) - n^2\Lambda(T) \tag{8}$$

where $e = P/(\gamma - 1)\rho$ is the internal energy, Γ and Λ are the heating and cooling rate, $\vec{\vec{\tau}}$ is the tensor of stresses which acts on the interface due to viscosity and ν is the coefficient of kinematic viscosity: $\tau_{ij} = \rho\nu\left(\frac{\partial v_i}{\partial x_j} + \frac{\partial v_j}{\partial x_i}\right)$.

3.2 Instability

For two incompressible, uniform fluids of constant density and viscosity separated by a horizontal boundary, Chandrasekhar [22] showed that the RT instability typical length is given by equation 9 [23].

$$\lambda_{max} = 4\pi\left(\frac{\nu^2 A}{g}\right)^{1/3} \tag{9}$$

where ν is the kinematic viscosity, g is the local gravitational acceleration, and A is the Atwood number $A = \frac{\rho_1 - \rho_2}{\rho_1 + \rho_2} = \frac{n_1 - n_2}{n_1 + n_2}$. n_1 and n_2 are the density of the heavier and lighter fluids respectively, in our case, the Galaxy and the HVC at the origin of the Draco nebula.

We will now estimate the relation between both densities. The kinematic viscosity ν can be express as $\nu = \frac{\mu}{\rho}$, where the dynamic viscosity μ is $\mu = \frac{1}{3}\frac{m\overline{v}}{\sigma}$, with the mean molecular mass m, the collision cross-section σ and $\overline{v} = \sqrt{\frac{8}{\pi}\frac{kT}{\mu_m m_H}}$. Therefore, we get $\nu = \frac{1}{3}\frac{1}{\sigma n}\sqrt{\frac{8}{\pi}\frac{kT}{\mu_m m_H}}$ and equation 9 gives equation 10:

$$\boxed{n_2 = \frac{T_1 - Bn_1^2}{T_1 + Bn_1^2} n_1} \tag{10}$$

$$B = \frac{\lambda_{max}^3 g}{(4\pi)^3}\frac{\pi \mu_1 m_H}{8k} 9\sigma^2$$

Chandrasekhar's study of hydrodynamic stability was made for the incompressible case. For the Draco nebula, both fluids are compressible. However, in 2004, Ribeyre et al. [24] studied the compressible case in supernovae. They compared with the incompressible case and found that compressibility has effects on the RT instability development. As expected, the RT instability growth is slower [24] but it has a similar λ_{max}.

Although there is no analytic description for the compressible case, the typical length of RT instability in supernovae is still estimated with equation 9 for supernovae remnant [23]. We will use the same approximation.

3.3 Local gravitational acceleration

The RT typical length (equation 9) depends on the local gravitational acceleration. Here, we estimate g for the Galactic disk. An alternative formulation of newtonian gravity is Gauss's law for gravity. It states that the acceleration $\overrightarrow{g}$ due to gravity of a mass m is given by:

$$\oiint_{\Sigma} \overrightarrow{g}.\overrightarrow{dS} = -4\pi G m$$

The circled integral sign indicates an area integral evaluated over a closed surface Σ. The vector $\overrightarrow{g}$ is the acceleration due to gravity, always pointing toward the mass. The vector $\overrightarrow{dS} = dS\hat{\mathbf{n}}$ is "normal" to the surface, pointing outward from Σ. m is the total mass inside Σ.

We assume the Galactic plane is assimilated to an infinite plane, having an area mass density $\sigma_m = \mu_1 m_H \, \Sigma_H$, where Σ_H is the mean surface density of hydrogen perpendicular to the Galactic disk and $\mu_1 m_H$ is the mean molecular mass in the Galaxy.

The appropriate gaussian surface Σ is a short cylinder whose flat faces (of area A) are parallel to the plane of mass. Everywhere along the curved surface of Σ, the gravitational acceleration $\overrightarrow{g}$ is perpendicular to the normal unit vector $\hat{\mathbf{n}}$ so the curved sides of Σ contribute nothing to the integral, only the flat ends of the cylinder do. On each end, g is anti-parallel to $\hat{\mathbf{n}}$ so $\overrightarrow{g}.\hat{\mathbf{n}} = -g$.

Applying Gauss's law, we get:

$$\iint_{\Sigma} \vec{g}.\overrightarrow{dS} = -g \iint_{+} \mathrm{d}S - g \iint_{-} \mathrm{d}S = -4\pi G m$$
$$-g(2A) = -4\pi G m \tag{11}$$

where signs + and − correspond to the upper and lower ends of the cylinder.

The mass m is equal to $\sigma_m A$ so the acceleration due to gravity is $\boxed{g = 2\pi G \sigma_m}$. It is independent of the distance from the plane. Finally, we get:

$$B = \frac{\lambda_{max}^3}{64\pi} \left(\frac{3\sigma}{2}\right)^2 \frac{G\Sigma_H}{k} (\mu_1 m_H)^2$$

3.4 Estimate of the typical length

We will now estimate λ_{max}. Using the column density map, we first estimated the angular size of the RT structures (figure 11). We found an average angular size of $\alpha = 10'.52$. We assumed the orientation of the structure has no influence on the size.

Thus, for a distance $d = 600\,pc$, the typical length of the RT instability structure is:

$$\lambda_{max} \sim \alpha d = \frac{10.52}{60} \frac{\pi}{180} 600 \approx 1.84\,pc$$

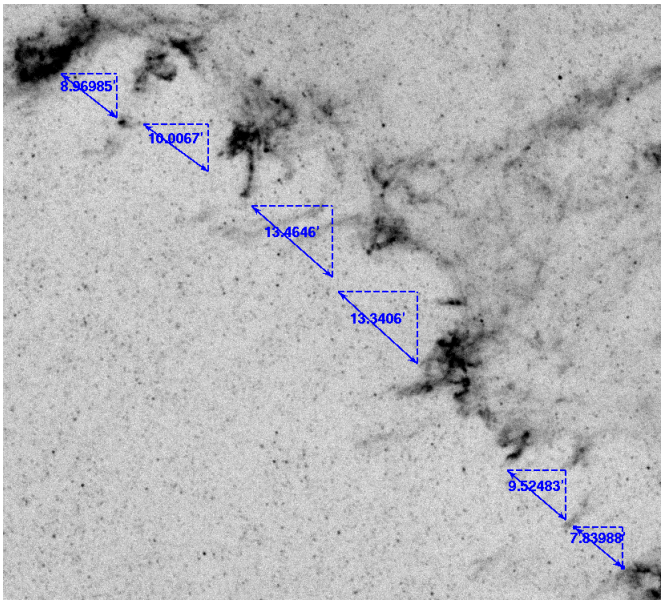

Figure 11: Rayleigh-Taylor instability structure as seen in the 250 μm SPIRE map. The blue arrows gives the apparent distance between fingers.

3.5 Numerical values of physical parameters

In 2008, Kalberla et al. [25] derived average surface densities perpendicular to the disk. It can be approximated over a broad radial range by exponential relations (figure 12). For the surface density, they found a scale length of 3.75 kpc within $12.5 \lesssim R \lesssim 30\ kpc$. For

$R \lesssim 12.5\ kpc$, the surface density is approximately constant.
The Draco nebula seems to be falling towards the inner Galaxy ($R \lesssim 8\ kpc$) so we adopt a surface density $\Sigma_H \sim 10^{21}\ cm^{-2}$.

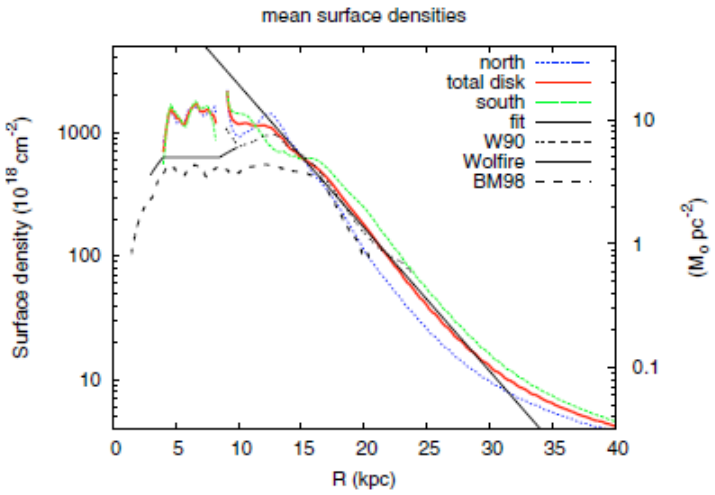

Figure 12: Derived mean surface densities of the HI gas perpendicular to the disk (red). The dotted blue line corresponds to the northern, the dotted green line to the southern part of the Milky Way. Figure from [25].

Collisional cross-section σ is defined as the area around a particle in which the center of another particle must be in order for a collision to occur. That area can change depending on the size of the two particles involved. Mathematically, it can be calculated using $\sigma = \pi(r_A + r_B)^2$. Assuming that both particles have the same radius and are hydrogen atoms, we get:

$$\sigma = \pi(2r)^2 \sim \pi(2 \times 5.3 \times 10^{-9})^2 \approx 3.53 \times 10^{-16}\ cm^2$$

The mean molecular weight μ_1 depends on gas metallicity. As we work with density of total hydrogen in any form, the mean molecular weight is $\mu_1 = 1.4$ [26]. Using the numerical values found above, we estimated that the coefficient B is equal to:

$$B \approx \frac{(1.84 \times 3.09 \times 10^{16})^3 \times (3 \times 3.53 \times 10^{-20})^2 \times 6.67 \times 10^{-11} \times 10^{25} \times (1.4 \times 1.67 \times 10^{-27})^2}{256\pi \times 1.38 \times 10^{-23}}$$

$$B \approx 6.77 \times 10^{-7}\ K.m^6$$

However, this value is very unprecise as it depends on the distance to the power 3 and the mean column density of the Galactic disk. From equation 10, we can find a condition on temperature and density in the Galactic disk:

$$T_1 - Bn_1^2 > 0$$

$$\frac{T_1}{n_1^2\ (cm^{-3})} > B \times 10^{12} \approx 6.77 \times 10^5\ K.cm^6$$

For typical value of temperature in the WNM [27], we may constrain the density:

$$n_1 < \sqrt{\frac{T_1}{B}} \approx \sqrt{\frac{8000}{6.77 \times 10^5}}$$
$$n_1 < 1.087 \times 10^{-1}\, cm^{-3}$$

Applying equation 10 with $n_1 \in [1 \times 10^{-3}; 0.108]$, we get figure 13. We found that the typical density of both fluids is $\sim 10^{-2} - 10^{-1}\, cm^{-3}$. They correspond to the density of the two media when the collision first occurs. The RT typical scale offers a way to go back in time, to the conditions that lead to the formation of dense clumps, dense enough to have strong CO emission.

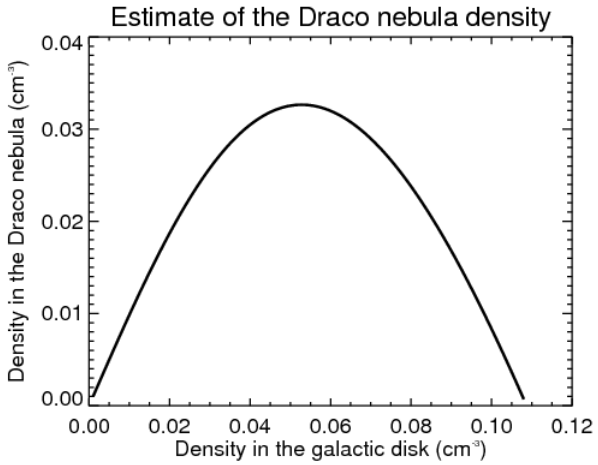

Figure 13: Density in the HVC vs density in the Galactic disk, assuming a temperature $T = 8000\, K$.

In the following, we investigate further the density and mass of those small scale structures.

4 Small scale structures

As seen before, the Draco nebula presents small scale structures (clumps) which are induced by the cloud collision with the disk. RT instability is characterised by gas fingers regularly spaced. When the fingers penetrate into the Galactic gas, the Kelvin-Helmoltz instability produces turbulence and forms clumps. With the increase in density, the WNM transits to CNM. The gas is then thermally stable in a cold and dense state. We will now focus on these clumps, studying their mass.

4.1 Source extraction

We first need to extract the clumps from the map of the Draco nebula. The extraction was made with the multi-wavelength source extraction code *GetSources* [28]. Designing automatic extraction codes is a complex task which was explored for a long time and is out of the scope of this work (collaboration with Vera Könyves). To decrease running time, *GetSources* was ran with a "mask" which limits the research area for extraction.

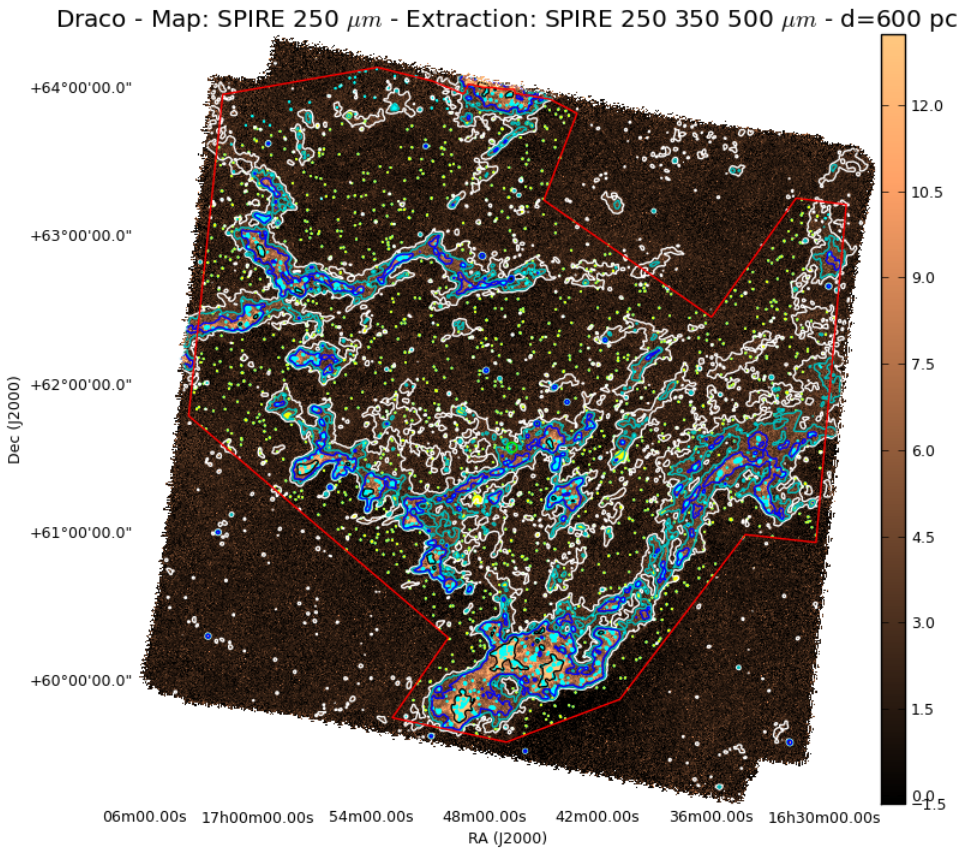

Figure 14: Representation of the sources on top of the dust emission map. Yellow → isolated sources; column density levels are (3.4×10^{20}, 5×10^{20}, 7.5×10^{20}, 2×10^{21} cm^{-2}).
The red contour represents the region where we made the extraction.

GetSources generates a catalogue of sources with a lot of features. Among that information, there are the coordinates; an estimate of the total flux of the sources in jansky

($1Jy = 10^{-26}\, W.m^{-2}.Hz^{-1}$) for each wavelength [1]; the major and minor axis of the elliptical footprint and how the ellipse is oriented on the sky.

I made a code to select the relevant sources, discarding the potentially spurious ones that are too close to the borders of the mask: 2375/2841 sources remain. The code also distinguishes the isolated sources (1536). Those sources are mostly background galaxies which are not differenciated by *GetSources*. Finally, the code plots the sources on top of the dust emission map (figure 14). At the end of this filtering, we have 839 sources.

4.2 Mass calculation

From the *GetSources* catalogue, we estimated the column density of the sources. We applied the same method as in part 2, assuming the temperature is the same along all the line of sight. The opacity was calculated with the calibrated flux at 250 μm: $\tau = \frac{I_{250}/cc}{B_{250}(T)}$.

Then, the mass is determined using formula 12 from [29]:

$$M = N_H\, \mu m_H\, \Omega\, d^2 \tag{12}$$

where Ω is the source solid angle of an elliptical footprint, μm_H is the mean molecular mass, d is the source distance and N_H is the mean column density.

As seen in part 1.3, distance is an important source of error. Indeed, distance estimate is not precised and distance appears to the power of 2 in equation 12.

4.3 Angular surface and density

The first analysis step I made was the angular surface distribution. *GetSources* catalogue gives the elliptical footprint caracteristics of the sources. I estimated the angular size as the area of the ellipse: $\Omega = \pi ab$. This analysis led to figure 15.

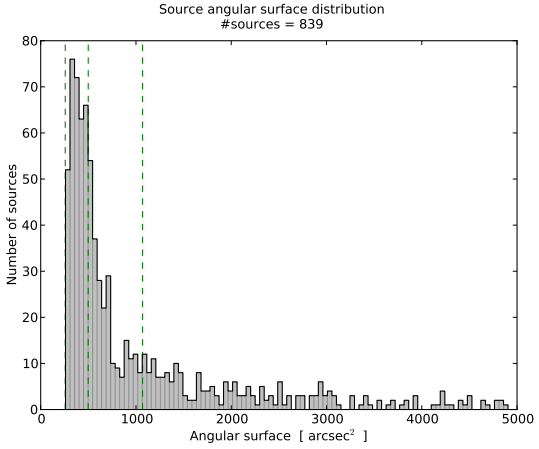

Figure 15: Surface distribution of the clumps in $arcsec^2$. The green dash lines indicate the beam solid angle.

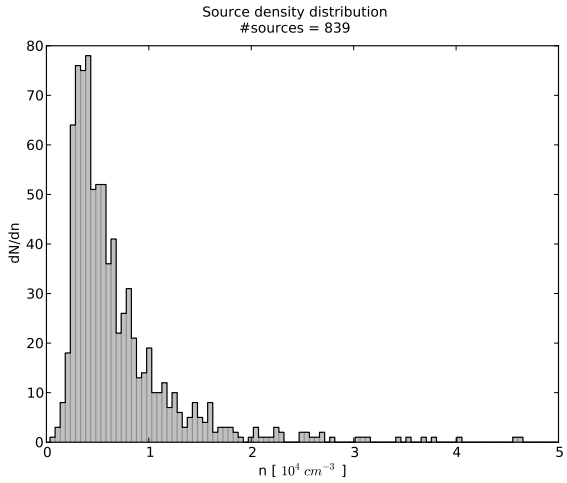

Figure 16: Density distribution of the clumps in units of $10^4 cm^{-3}$.

[1] Despite the offset of intensity in *Herschel* maps, *GetSources* is able to compute the absolute flux of sources.

Using this area, we estimated the efficient radius R_{eff} of the ellipse. It corresponds to the radius of the circle which has the same area: $R_{eff} = \sqrt{ab}$. Assuming the sources to be spherical clumps, their mass density is $\rho = \frac{M}{\frac{4}{3}\pi R_{eff}^3}$. Figure 16 is the distribution of density $n = \rho/\mu m_H$.

As expected, the minimum angular size is limited by the size of the beam at 250 μm. Most of the sources are resolved at 250 and 350 μm but only a few are resolved at all SPIRE wavelength. In addition, the mean density of the clumps is $\langle n \rangle \sim 7 \times 10^3\ cm^{-3}$. This is 5-6 order of magnitude greater than the initial densities of the colliding fluids. The value we found is in agreement with the fact that CO emission is observed.

4.4 Clump mass function

Integrating the column density deduced from dust emission over the whole nebula, the total mass of the Draco nebula is estimated to be $\sim 8 \times 10^3\ M_\odot$. The total amount of mass in the clumps is $\sim 1.1 \times 10^3\ M_\odot$. We will now study the clump mass function (ClMF). From the *GetSources* catalogue, we can draw the histogram of the mass distribution of the sources (figure 17). The distribution follows a power law for masses between 0.3 $M_\odot$ and 50 $M_\odot$.

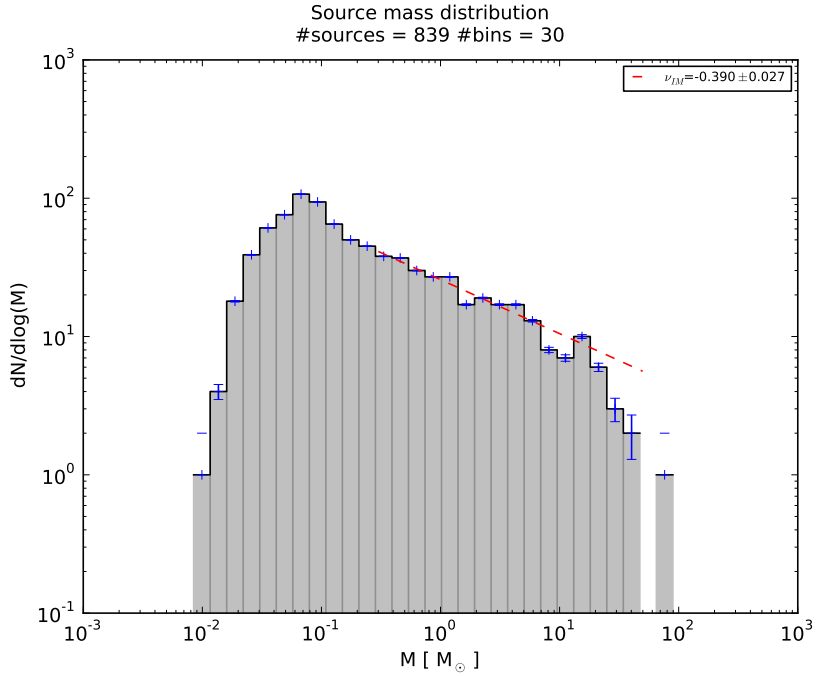

Figure 17: Mass distribution of the clumps. The red dash lines is the fit plot of the power law.

Taking in account statistical error bars in $1/\sqrt{N}$, I fitted a power law in linear scale, which correspond to a linear law in logarithm scale. The power index value is given with a small incertainty (-0.390 ± 0.027). However, we do not find the same value when we take a different number of bins. To get a better idea of the uncertainty, I made many histograms changing the number of bins and found a slope in the range $-0.36 > \nu_{IM} > -0.49$.

5 Discussion

5.1 Jeans mass

Jeans mass is defined as $M_J = \left(\frac{1}{\mu m_H}\right)^2 \left(\frac{5}{2}\frac{kT}{G}\right)^{3/2} \left(\frac{4}{3}\pi n\right)^{-1/2}$. This is the maximal mass of stable isolated and spherical clouds. The mean molecular weight is $\mu \approx 1.4$ and Jeans mass is defined by [27]:

$$M_J \approx 5.6 \left(\frac{T}{10\ K}\right)^{3/2} \left(\frac{n}{10^4\ cm^{-3}}\right)^{-1/2} M_\odot \tag{13}$$

Applying equation 13 and assuming dust and gas in thermal equilibrium (i.e. that dust temperature is similar to gas temperature with $T_d \sim 17-22K$, we calculated the Jeans mass for all the sources. Plotting the mass versus the Jeans mass (figure 18), one may determine if the sources are self-gravitating. All the sources which are above the $y = x$ line are self-gravitating. In total, we found 25 out of 839 sources with masses greater than their Jeans mass. This result clearly shows that the clumps seen in Draco are not the result of gravity but are rather the result of the dynamical instabilities in the shock front.

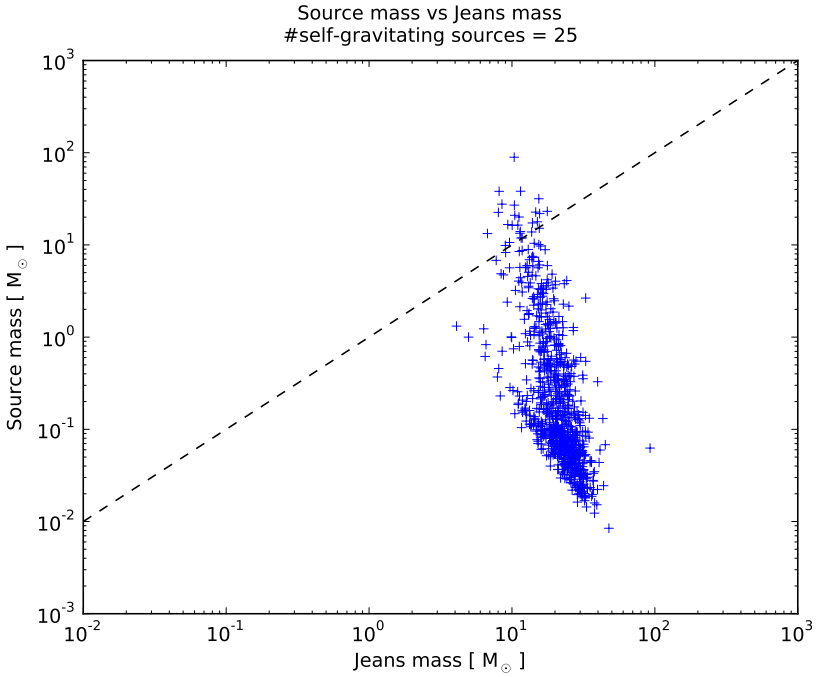

Figure 18: Mass of the sources vs the Jeans mass. The black dash line corresponds to $y = x$.

5.2 The clump mass functions

In 2013, Veltchev et al. [30] statistically derived the clump mass function and compared it with mass distributions of clumps from dust continuum maps of molecular clouds complexes (eg. Taurus, Orion). They found two power laws regimes at intermediate ($< 200 - 300\ M_\odot$) and high masses ($> 200 - 300\ M_\odot$). For the intermediate masses part of the ClMF, these authors found a slope $-0.25 > \nu_{IM} > -0.55$. They found a higher slope for high masses: $-0.9 > \nu_{HM} > -1.6$.

The values we found in part 4.4 are similar to those obtained by Veltchev et al., keeping in mind that the slope depends on the number of bins. The slope found by Veltchev et al. [30] for high masses probably comes from gravitational process as it is similar to the slope of the CMF and IMF (see pert 5.3).

5.3 Relation with the core and initial mass functions

We will now investigate the relation between the ClMF and the CMF. In 2010, Könyves et al. [31] worked on the prestellar population in the Aquila cloud. They extracted the sources with *GetSources*. Using $1/\sqrt{N}$ statistical uncertainties, these authors got the CMF in figure 19.

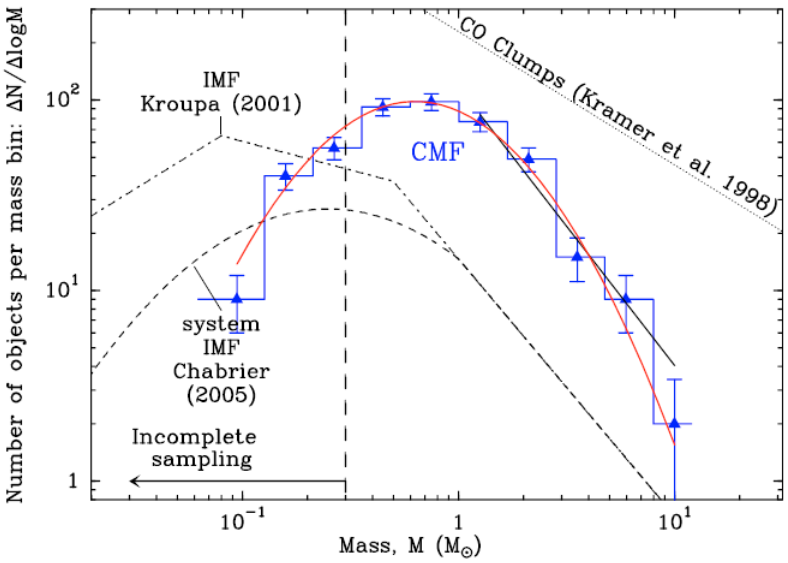

Figure 19: Differential mass function of 452 starless cores in the Aquila cloud. The red curve is a lognormal fit, and the high-mass end is fitted by a power law. The dash-dotted line shows the Kroupa 2001 IMF, and the dashed curve corresponds to the Chabrier 2005 IMF.

They fitted a power law for high masses and found a slope $\nu_{CMF} = -1.5 \pm 0.2$. This slope is similar to that of the IMF: $\nu_{IMF} = -1.35$. There is a factor of 3-4 between our value for the ClMF and those of the CMF/IMF. This result highlights the fact that the formation processes are not the same. Stars and cold cores are formed by gravity, contrary to the clumps in the Draco nebula which are formed by instabilities (Rayleigh-Taylor, Kelvin-Helmoltz and thermal instabilities).

Conclusion

I have worked on *Herschel*-SPIRE observations of the Draco nebula. Draco is a diffuse high Galactic latitude interstellar cloud located about 370 pc above the Galactic plane. The formation of the Draco nebula is still uncertain. The favored scenario is a collision between a high-velocity cloud and the warm neutral medium of the Galactic disk. The HVC is of extragalactic origin and is falling towards the Galactic disk.

I combined the *Herschel* data with *IRAS* and *Planck*, and HI-21 cm data in order to study the gas dynamics and the properties of the nebula. Using a model of big dust grains emission and a dust temperature map from the *Planck* archive ($5'$ resolution), I computed a map of total hydrogen column density at $17.6''$ resolution using the SPIRE 250 μm map.

The high resolution of SPIRE data reveals a Rayleigh-Taylor (RT) instability structure at the hypothetic shock-front. I studied the RT instability theory in the case of Draco. Using a simple equation between the typical length of RT structure and both fluids densities, I found that the HVC and the WNM at the origin of the Draco nebula were very diffuse ($n \sim 10^{-2} - 10^{-1}\ cm^{-3}$). Due to the collision, dense clumps were formed by Rayleigh-Taylor and Kelvin-Helmholtz instabilities. Those clumps are now dense enough to have strong CO emission.

The clumps were extracted from the SPIRE data using the code *GetSources* which generates a catalogue of sources. Filtering the catalogue, we finally have 839 relevant sources. Applying the same method used to compute the column density map, we estimated the column density and mass of the sources. We found that 1/8 of the Draco nebula mass is located in clumps.

The clump mass function follows a power law: $-0.36 > \nu > -0.49$. This index is compatible with the one of non self-gravitating clumps observed in molecular clouds like Taurus or Orion. On the other hand, this a factor of 3-4 smaller than the slope of the core and initial mass function, for which gravity plays an important dynamical role.

Of the 839 sources, we found only 25 sources with masses greater than their Jeans mass. These results clearly shows that gravity is not a dominant process in the clumps formation.

The processes involved in the formation of Draco (turbulence, magnetic field, heating/cooling processes) are complex and not well understood. Nevertheless, the results presented here provide interesting avenues that could be explored further using numerical simulations. This is out of the scope of my internship but would be explored later.

References

[1] *The Accretion of Fuel at the Disk-Halo Interface*, Putman et al. 2009, EAS Publications Series.

[2] *Cold gas accretion in galaxies*, Sancisi et al. 2008, A&A review.

[3] *The Evolution of Gas Clouds Falling in the Magnetized Galactic Halo: High-Velocity Clouds (HVCs) Originated in the Galactic Fountain*, Kwak et al. 2009, ApJ.

[4] *The Draco nebula: A molecular cloud in the galactic halo?*, Mebold et al. 1985, A&A.

[5] *A high latitude HI-cloud with optical emission*, Goerigk et al. 1983, A&A.

[6] Planck *early results. XXIV. Dust in the diffuse interstellar medium and the Galactic halo*, Planck Collaboration 2011, A&A.

[7] *Physical properties of a very diffuse HI structure at high Galactic latitude*, Miville-Deschênes & Martin 2007, A&A.

[8] *Hydrodynamical processes in the Draco molecular cloud*, Odenwald & Rickard 1987, ApJ.

[9] *Collision of a high-velocity cloud with a dust cloud in the Galactic halo*, Rohlfs et al. 1989, A&A.

[10] *A neutral gas jet in a low velocity shock front at the boundary of the Draco Nebula*, Kalberla et al. 1984, NASA Conference Publication.

[11] *A* Far Ultraviolet Spectroscopic Explorer *survey of molecular hydrogen in Intermediare-Velocity Clouds in the Milky Way halo*, Richter et al. 2003, ApJ.

[12] *X-ray shadows of the Draco nebula. A new method to determine total hydrogen column densities*, Moritz et al. 1998, A&A.

[13] *Molecular gas at high Galactic latitudes*, Magnani et al. 1985, ApJ.

[14] *Molecular Cloud Formation in Shock-compressed Layers*, Koyama & Inutsuka 2000, ApJ.

[15] *The distance of the Draco Nebula and its high velocity clouds*, Goerigk & Mebold 1986, A&A.

[16] *Interstellar NaID line studies of stars towards the Draco nebula*, Lilienthal et al. 1991, A&A.

[17] *The Distance to the Draco Intermediate-Velocity Cloud*, Gladders et al. 1998, ApJ.

[18] *H I in the Galaxy*, Dickey & Lockman 1990, Annual Review A&A.

[19] Planck *early results. XIX. All-sky temperature and dust optical depth from* Planck *and IRAS. Constraints on the "dark gas" in our Galaxy*, Planck Collaboration 2011, A&A.

[20] *IRIS: a new generation of* IRAS *maps*, Miville-Deschênes & Lagache 2005, ApJ.

[21] *The dust/gas correlation at high Galactic latitude.*, Boulanger et al. 1996, A&A.

[22] *Hydrodynamic and hydromagnetic stability*, Chandrasekhar 1961, Oxford University Press.

[23] *A Case Study of Small-scale Structure Formation in Three-dimensional Supernova Simulations*, Ellinger et al. 2012, ApJ.

[24] *Compressible Rayleigh-Taylor instabilities in supernova remnants*, Ribeyre et al. 2004, Physics of Fluids.

[25] *Global properties of the H I distribution in the outer Milky Way. Planar and extra-planar gas*, Kalberla & Dedes 2008, A&A.

[26] *Allen's astrophysical quantities, 4th ed.*, Cox 2000, New York: AIP Press; Springer.

[27] *The Interstellar Medium*, Lequeux 2005, EDP Sciences.

[28] *A multi-scale, multi-wavelength source extraction method:* getsources, Men'shchikov et al. 2012, A&A.

[29] *The Mass Distribution and Lifetime of Prestellar Cores in Perseus, Serpens, and Ophiuchus*, Enoch et al. 2008, ApJ.

[30] *Clump mass function at an early stage of molecular cloud evolution - II. Galactic cloud complexes*, Veltchev et al. 2013, Monthly Notice of the Royal Astronomical Society.

[31] *The Aquila prestellar core population revealed by* Herschel, Könyves et al. 2010, A&A.

An all-sky model of the dust emission based on the Planck *and* IRAS *data*, Planck collaboration 2013, in preparation

Acknowledges

First of all, I thank my internship supervisor Marc-Antoine. Thank to him, I learnt a lot of new things about interstellar medium. He also contributed to the fact I want to continue my studies with a PhD in interstellar medium.

Then, thank to the people of MIS research group of IAS, in particular the MISTIC group, for their friendship. I did feel like a member of the research group with them, instead of an intern.

Finally, I thank Vera Könyves who helped us running the code *GetSources* in CEA. Without her, we would not be able to run the code and make a proper extraction.